Initial stages of water adsorption on NaCl (100) studied by scanning polarization force microscopy

Albert Verdaguer, G. M. Sacha, M. Luna, D. Frank Ogletree, and Miquel Salmeron[a)]
Materials Sciences Division, Lawrence Berkeley National Laboratory, Berkeley, California 94720

(Received 11 February 2005; accepted 15 June 2005; published online 23 September 2005)

Scanning polarization force microscopy was used to study the topography, polarizability, and contact potential of cleaved NaCl(100) as a function of the relative humidity (RH) between <5% and 40%. In this humidity range there are reversible changes in surface potential and polarizability, while large scale modifications in step topography and irreversible ion redistribution occur above 40% RH. In dry conditions the surface contact potential was more negative near atomic steps than over flat terraces. As humidity was increased, changes were observed in the local polarizability of the steps due to ionic solvation, and the contact potential of the terraces became more negative. At 40% RH surface-potential differences between steps and terraces could no longer be detected. These results are interpreted in terms of preferential anion solvation, initially localized near steps, and later spreading over the entire surface. © *2005 American Institute of Physics*. [DOI: 10.1063/1.1996568]

I. INTRODUCTION

Adsorption of water on salt crystals plays a key role in several atmospheric and environmental processes. Micrometer and submicrometer crystals of sodium chloride (and, to lesser extent, other alkali halides) are major constituents of atmospheric aerosols. These aerosols play an important role in drop nucleation in clouds.[1] Important chemical reactions among atmospheric components take place on the surfaces of saline droplets.[2] We have investigated the initial stages of the dissolution process on NaCl crystals, including the role of surface defects such as steps.

In the last years the development of noncontact scanning microscopy techniques based on the atomic force microscope (AFM) using electrostatic forces has made possible the study of soft surfaces, in particular, liquid films and droplets, with minimum perturbation. This operation mode, which we call scanning polarization force microscopy (SPFM), has already been applied to the study of water adsorption on alkali halides.[3,4] The SPFM provides information on surface topography, dielectric properties, and contact potential variation.

Previous macroscopic studies[5] of the electrical properties of cleaved NaCl exposed to water vapor found that there was a characteristic relative humidity (RH) value of ~40% that separated two water adsorption regimes. Infrared studies suggest that the first regime corresponds to a water coverage between zero and one monolayer.[6] In this regime only small modifications of the step structure were observed by AFM.[3] In the second regime, between 40% and 75% RH, large scale modifications of the step structure were observed, followed by deliquescence of the crystal at 75% RH. Using SPFM, Luna *et al.*[4] found that for NaCl there was a substantial change in the rate of increase of ionic mobility and surface potential at the "critical" humidity of ~40%. Recent work on Br-doped NaCl has shown that irreversible changes take place in surface structure and ion distribution when alkali halide surfaces are exposed to humidity above the critical value.[7] In this paper we will focus on the adsorption of water on NaCl below the critical humidity. We extend previous work on the contact potential of NaCl (100)[4,5] that was performed averaging over the surface, which did not permit separation between step and terrace contributions. Spatially resolved frequency-dependent images allow us to correlate the previously reported changes in polarizability with ionic mobility at the steps.

A. SPFM operation

The operation in the SPFM mode has been described elsewhere[8,9] and therefore only a brief description is given here. To perform noncontact electrostatic AFM imaging, a conductive tip is electrically biased to a few volts, creating attractive electrostatic forces between the tip and the surface. The electrostatic force can be written as

$$F_e(V) = aV^2 + bV + c, \tag{1}$$

where a, b, and c are factors which depend on tip shape, tip-sample separation, and sample polarizability.[10] The quadratic term is due to the polarization of the sample by the biased tip (induced charges), and the remaining terms describe the interaction between the biased tip and charges or dipoles preexisting on the surface. The voltage applied to the tip is of the form:

$$V = V_{dc} + V_{ac}\sin(\omega t). \tag{2}$$

The frequency ω can be varied to explore time-dependent phenomena.[11] In our studies, the tip-sample separation was 10–50 nm, the amplitude V_{ac} was varied between 5 and 12 V, and the frequency ω between 40 Hz and 4 kHz. Inserting expression (2) in (1), we obtain contributions to the electrostatic force at the first and second harmonics of ω, F_ω, and $F_{2\omega}$, as well as a dc term F_{dc}. In SPFM the second

a)Electronic mail: mbsalmeron@lbl.gov

harmonic term $F_{2\omega}=\frac{1}{2}aV_{ac}^2$ is used for feedback control. A feedback loop maintains the amplitude of the 2ω component of the lever oscillation (detected by a lock-in amplifier) constant by controlling the z piezodisplacement. The information on topography and sample polarizability are mixed in images based on detecting $F_{2\omega}$.[12] In spite of this we will refer to such images as "topographic" for brevity.

The first harmonic term F_ω is proportional to the tip-sample contact potential difference. A second feedback loop adjusts V_{dc} to null the F_ω component, thus providing a direct measurement of the tip-surface contact potential difference V_c.[13] This is a nanometer-scale version of the macroscopic Kelvin probe method that has been used by many authors in the past.[13] We will refer to the V_{dc} images obtained by nulling the 1ω signal as Kelvin probe (KP) images. In our variable-humidity experiments, the observed contact potential changes are due to the sample, since the tip was made hydrophobic by coating it with silane molecules. The tip passivation was always checked by measuring the humidity-dependent contact potential difference with a clean highly ordered pyrolytic graphite (HOPG) surface whose contact potential is independent of humidity. Only coated tips showing a constant contact potential were used in the salt experiments.

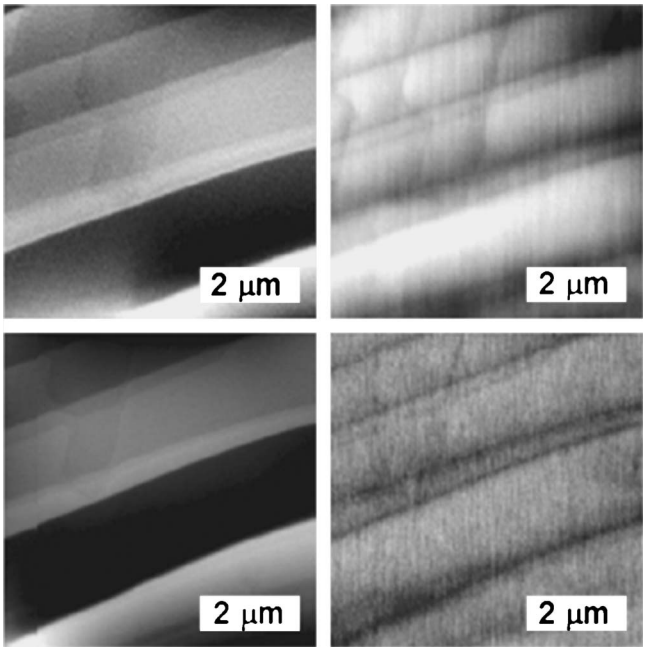

FIG. 1. Top: SPFM images of a NaCl surface prepared by cleavage in 12% RH. Left: topographic image. Right: contact potential image acquired simultaneously. Surface steps appear as dark lines in the contact potential image, indicating that they are more negative than the terraces. The terrace contact potential is not homogeneous. Bottom: the same area at 25% RH. Left: SPFM topography. Right: contact potential. At this humidity the contact potential differences inside the terrace have disappeared and only the step contrast remains. Gray scales are 5 nm for the topographic images and 50 mV for the contact potential images (bright to dark).

II. EXPERIMENT

All the experiments were carried out at room temperature (21 ± 1 °C) with a home-built AFM[14] and a commercial SPM100 electronic control from RHK Technology, Inc. The microscope head was enclosed in a glove box. Humidity control was achieved by circulating dry N_2 to decrease RH or by bubbling N_2 through de-ionized water to increase RH. RH was measured using an Omega hygrometer. The values from 5% to 40% RH could be maintained inside the microscope enclosure with a humidity variation less than $\pm1\%$ per hour. The absolute RH values have an uncertainly of $\pm5\%$.

Most of the NaCl crystals used in the experiments were grown from the melt by the Crystal Growth Laboratory of the University of Utah in Salt Lake City. We also used also natural crystals,[15] which had a purity of 99.9%, with Ca being the most common impurity. The natural crystals showed also a small haziness, probably due to air inclusions. Synthetic crystals grown from the melt have a higher purity (99.999%)[7]and showed no visible inclusions. X-ray photoemission spectroscopy (XPS) analysis showed pure NaCl for both types of crystals within the detection limits of the technique ($\sim0.5\%$). As we discuss below, the use of these two types of crystals helped to clarify differences among the present results, obtained with the melt-grown crystals, and previous results, obtained with less pure crystals.

The single crystals were cleaved parallel to the (100) plane inside the AFM glove box at low humidity (10% RH), and never exposed to water vapor above the critical humidity. The AFM cantilevers (Molecular Imaging-Nanosensors), were coated with 5 nm of Ti followed by 50 nm of Pt and had a spring constant of 0.5 N/m and a resonant frequency around 11 kHz.

III. RESULTS

A. Difference in surface-potential contrast of natural and melt-grown crystals

After cleavage at low humidity the crystal surfaces were always electrically charged. The surface-potential difference measured a few minutes after cleavage often exceeded 10 V, either positive or negative. The strong electrostatic interaction between the tip and the sample prevented useful measurements under these conditions. The large initial surface potential decreased with time, probably due to radiation and adsorption of water molecules, even at low humidity. Experiments were started only after the contact potential stabilized, typically within 30 min. The contact potential at this point varied from a few tens to a few hundreds of millivolts, more often negative relative to the tip.

Topographic SPFM images acquired at low humidity (10%–25%) show straight steps in [010]-type directions (Fig. 1, left). Some curved steps were also observed. The KP images obtained simultaneously showed a contact potential difference between the steps and the terraces. Unexpectedly, the sign of the potential difference depended on the purity of the salt samples. For the natural crystals, the steps were found to be more positive than the terraces, in agreement with the previous work.[4] In contrast, for the melt-grown crystals, a more negative step potential was always found. The negative step potential for the melt-grown crystals was clearly

TABLE I. Difference between contact potential on the terraces and on the steps for different step heights at a relative humidity of 25%.

Step height (nm)	0.26	0.58	1–2	>5
No. Atoms/step	1 atom	2 atoms	3–8 atoms	>20 atoms
ΔV (mV)	−15±5	−25±5	−35±5	−40 to −100

resolved for steps of all heights (monoatomic to multiatomic), while for natural crystals the positive step potential could only be clearly resolved for large, multiatomic steps.

After exposure to RH above the critical value of ~40%, irreversible ionic redistribution can take place, and after returning to low RH the surface potential can vary in sign and magnitude from step to step and even from terrace to terrace.[7] Therefore, the results presented here are confined to melt-grown crystals that were never exposed to humidity above 40%.

B. Contact potential versus relative humidity

At low humidity (Fig. 1, top right), terraces showed contact potential variations (within ±100 mV) with no clear correspondence to any topographic features (Fig. 1, top left). These differences decreased with increasing RH and disappeared at approximately 25% RH (Fig. 1, bottom right). At this point the contact potential became uniform across the terraces, and only the potential difference between steps and terraces could be observed. We also found that the contact potential of the steps relative to the terraces was fixed for a given humidity, and increased with step height, being more negative for the higher steps. The ratio was not linear with step height, as shown in Table I.

Using macroscopic Kelvin probe techniques, the previous work has shown that the NaCl surface is negatively charged after cleavage in UHV.[16] These studies found that the contact potential on large macroscopic steps was always more negative than on flat areas. It is known that at the surface of ionic crystals there is an electric dipole layer, the Debye-Frenkel double layer, which is due to an imbalance between cation and anion concentrations. The imbalance originates from the difference in the formation energies of cation and anion vacancies.[17] This effect is more important when defects such as steps are present on the surface.[17] The macroscopic observations agree with theoretical predictions[16] of negative surface charge. Our observations show that this charge is inhomogeneous on the nanometer scale. Excess of charge of one sign can exist in localized regions, for example, at steps, but also within single terraces. As the humidity increases, the terrace charges become homogeneous, probably due to water facilitating the diffusion of surface ions. The negative potential of the steps relative to the terraces persisted at this humidity.

Figure 2 shows topographic and contact potential profiles across two steps: a large one 6.5 nm high (~25 monolayers) can be seen close to a monoatomic step of 0.26 nm. At 30% RH the contact potential difference V_c was +75 mV

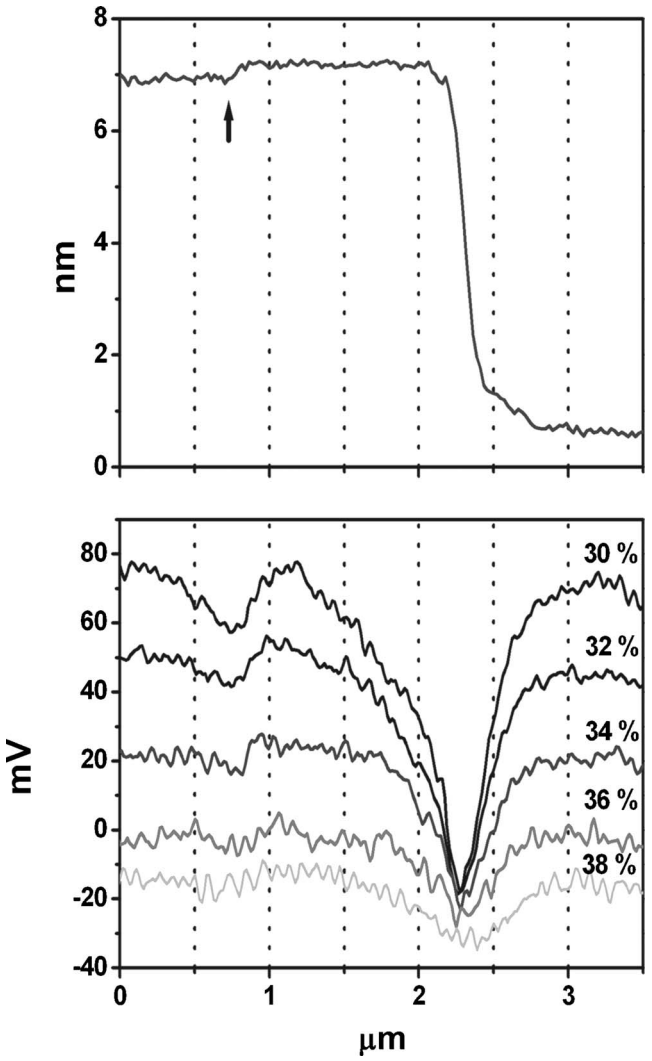

FIG. 2. Top: topographic profile showing a multiple step 6.5 nm high and a monoatomic step (marked by an arrow) at 30% RH. Bottom: contact potential of the same area for different humidity values.

over the terraces. At the monoatomic step V_c was +60 or −15 mV relative to the terrace, and at the large step V_c was −10 or −85 mV relative to the terrace.

Changes in contact potential were measured as RH approached the critical value of 40% with the tip repetitively scanning along the same line (Fig. 2, bottom panel). A monotonic decrease of the contact potential at the terraces and monoatomic steps was observed. In contrast, the value of the potential at large steps did not change substantially. Another important finding was that the potential difference between terraces and steps decreased as humidity increased. At 38% RH the potential difference was barely detectable, and it completely disappeared for ⩾40%.[4,7] When RH was kept below 40% the observed potential changes were completely reversible.

C. Ion mobility

The 2ω amplitude used for the z piezofeedback contains both topographic and polarizability informations. As we shall show, humidity causes ionic solvation, which increases the polarizability of the surface due the mobile nature of the

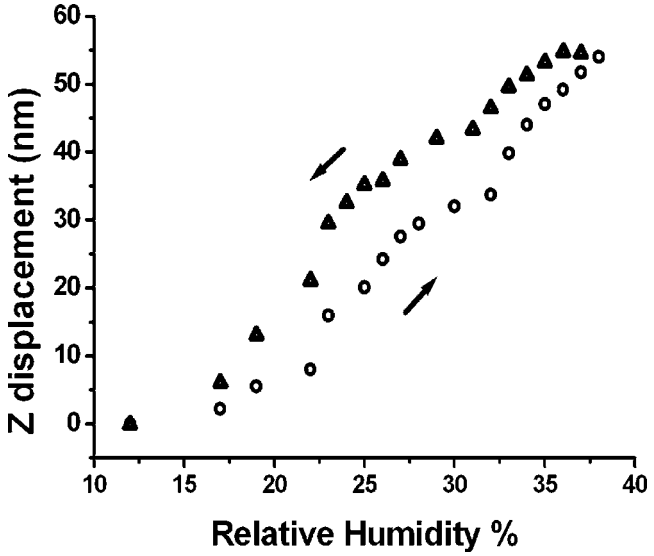

FIG. 3. Increase in tip-sample separation (z displacement) as a function of relative humidity. The change in z is due to the increasing polarizability of the surface that increases the electrostatic force at a given distance as the humidity increases.

solvated ions. An illustration of this effect is shown in Fig. 3, where the z displacement of the tip, located at a fixed point over a terrace, is plotted against RH. From 12% to 38% RH a total displacement of about 50 nm was observed (for $V_{ac}=12$ V and $\omega=4$ kHz). When the humidity decreased, the original position was recovered. This z displacement was due purely to the increase in surface polarizability, which increases the electrostatic force, causing the feedback loop to retract the tip to maintain a constant 2ω amplitude. Since the spatial resolution of the topographic images depends on the tip-sample distance, this effect needs to be taken into account when acquiring images at different humidity values. We accomplished this by readjusting the amplitude set point so as to maintain similar imaging distances and resolution for different RHs.

The increase in surface polarizability upon water adsorption is inhomogeneous, being stronger at the steps, which leads to an enhancement of contrast in the SPFM images, as shown in Fig. 4. No enhancement was observed in contact AFM images acquired under the same conditions. A similar step enhancement was reported previuosly,[4] but the origin of the enhancement was not determined. We now discuss this interesting effect in more detail.

In Fig. 4 we show simultaneously acquired topographic and KP images of NaCl. The top image, at 25% RH, shows monoatomic steps with rounded edges resulting from water exposure. The KP image reveals the more negative potential at the steps. When the RH increases to 30% (middle image), a topographic enhancement is observed at some steps, while the contact potential difference decreases, as described in the Sec. III B. When RH reached 35% the topographic enhancement of the steps was several nanometers, producing the bright decoration in the images. The KP image shows a reduction of the potential difference between steps and terrace at this point.

Frequency-dependent SPFM imaging was used to determine whether the step enhancement in the topographic images is a geometrical effect, due, for example, to a ribbon of adsorbed water decorating the steps or an electrical effect of higher polarizability at the steps, due, for example, to the enhanced mobility of solvated ions. In Fig. 5, we show two topographic images at 34% RH, at frequencies of 4 kHz (left) and 400 Hz (right). It is clear that step enhancement is much lower for the 4 kHz than for the 400-Hz image. This observation rules out the geometrical explanation of a water ribbon. If adsorbed water decorated the steps, the observed height should be independent of frequency since water dipoles have a frequency response in the gigahertz range. We attribute the observed enhancement to the increased mobility of solvated ions at the steps, diffusing in response to the electric field of the tip with time constants in the millisecond range. No enhancement was observed below 30% RH, even at frequencies as low as 40 Hz.

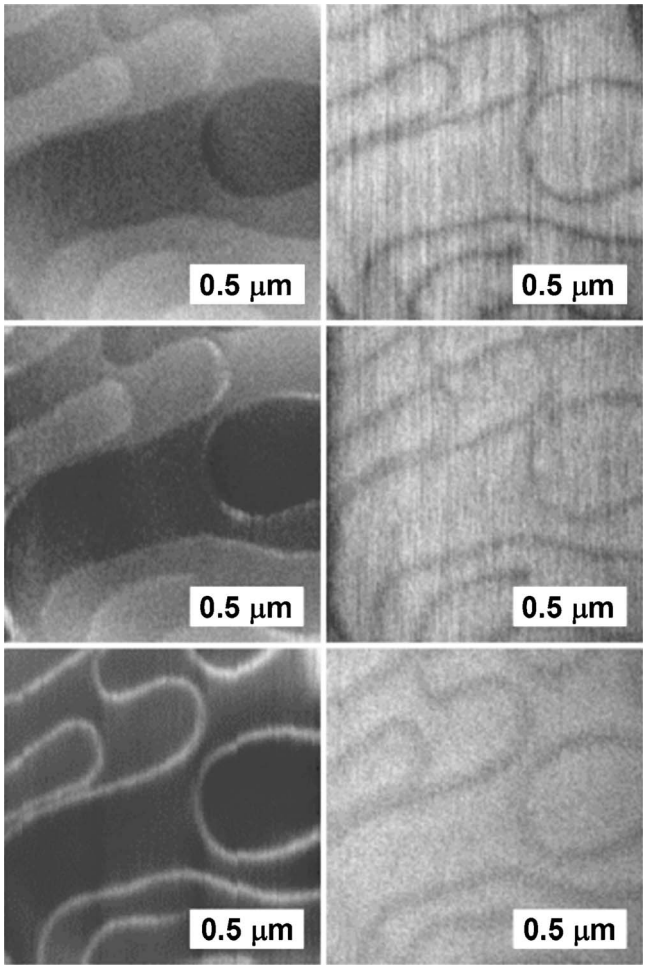

FIG. 4. SPFM topographic (left) and contact potential (right) images acquired at different RH values. The images at the top correspond to RH =25%. The middle images, acquired at 30% RH, show a moderate enhancement of the step contrast. At 35% RH (bottom images) the step enhancement is large (several nanometers). At the same time the contrast of the steps in the contact potential images relative to the terraces decreases with humidity, Gray scales are l0 nm for the topographic images and 50 mV for the contact potential images (bright to dark).

We also followed the evolution of a topographic line profile in the same region as in Fig. 3, containing a monoatomic step and a large step, as the humidity changed from

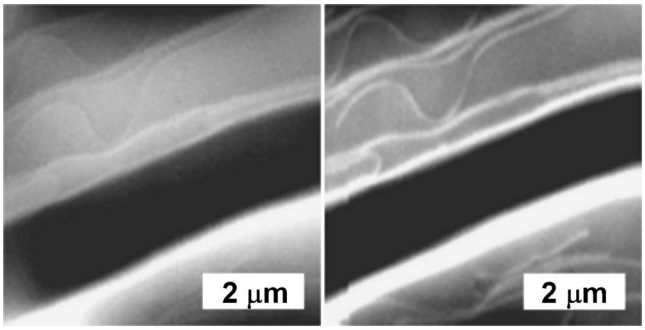

FIG. 5. SPFM images of a NaCl surface at 34% RH. The frequency of the ac-bias applied to the tip was 4 kHz in the left image and 400 Hz in the right one. A contrast enhancement can be seen at the steps in both cases, but the enhancement is much larger in the image acquired at the lower frequency. (Gray scale of 10 nm, bright to dark).

30% to 38% and back to 30%. The results are shown in Fig. 6 for frequencies of 40 and 400 Hz and 4 kHz. Not only was there an enhancement off the step height, but as the humidity approached 40% the topographic enhancement started to spread over the entire surface, as can be seen by the widening peak of the step profile. At 40% RH (and above) the enhancement was uniform over the entire surface.

IV. DISCUSSION

A. Melt-grown versus natural crystals

The difference in the polarity of the contact potential at the steps relative to the terraces observed for melt-grown and natural crystals was unexpected and difficult to understand. We propose the following scenario to explain our observations. We assume that the differences between the two crystals must be related to the presence of impurities and to the ease of ion vacancy formation and of solvation and dissolution when exposed to humid air. Unfortunately it is impossible with our instruments to detect and quantify composition differences below surface concentrations of 0.01 monolayer. However, electrostatic effects are extremely sensitive to small imbalances in surface charge. For example, displacing 0.01 monolayer of monovalent ions by by 0.1 nm perpendicular to the surface, forming a dilute dipole layer, would produce a change in contact potential on the order of 1 V. Since the potential changes observed in our experiments are less than 0.1 V, it is quite likely that the concentration of displaced impurity ions is on the order of 10^{-3} monolayer. Careful analysis of the results of Luna *et al.*[4] reveals that for the various alkali halide crystals used, after an initial increase in contact potential with increasing humidity, most crystals then showed either an absolute decrease in contact potential after the critical humidity (point A in Ref. 4), or a decrease in the slope. In light of the results obtained with high-purity, melt-grown crystals, we propose that solvation occurs first for impurity cations at step edges, then for majority anions, and finally for majority cations. For natural crystals, step cation impurity vacancies lead to a positive step potential under dry conditions, while for ultrahigh-purity crystals anion vacancies are dominant, leading to a negative step potential. The irreversible changes in contact potential after exposure to RH above the critical value are probably due to kinetic effects. Once the critical humidity value has been reached, a substantial fraction of surface anions and cations have become solvated. When RH is reduced, water desorbs from the surface and the anions and cations must find new lattice sites. Surface-potential variations, often with randomly distributed positive and negative steps and terraces and irregular step structures are the result of imperfect equilibration due to fast evaporation.

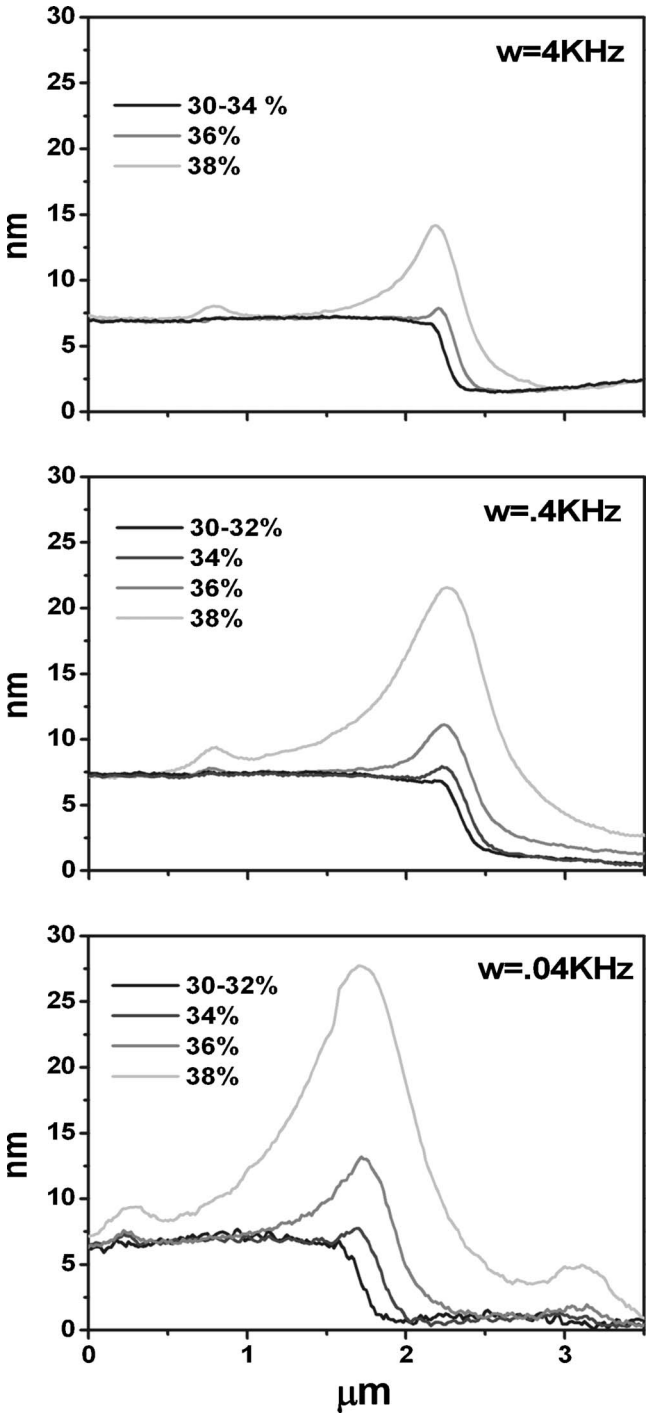

FIG. 6. SPFM topographic profile of the same step region as in Fig. 3, acquired at different frequencies and different RHs. An increase of the apparent height of the step can be observed as RH increases. The effect is stronger at low frequencies. This is attributed to moving charges (solvated ions) that increase the polarizability at the steps. At high humidity the mobile charges spread from the steps to the adjacent terraces.

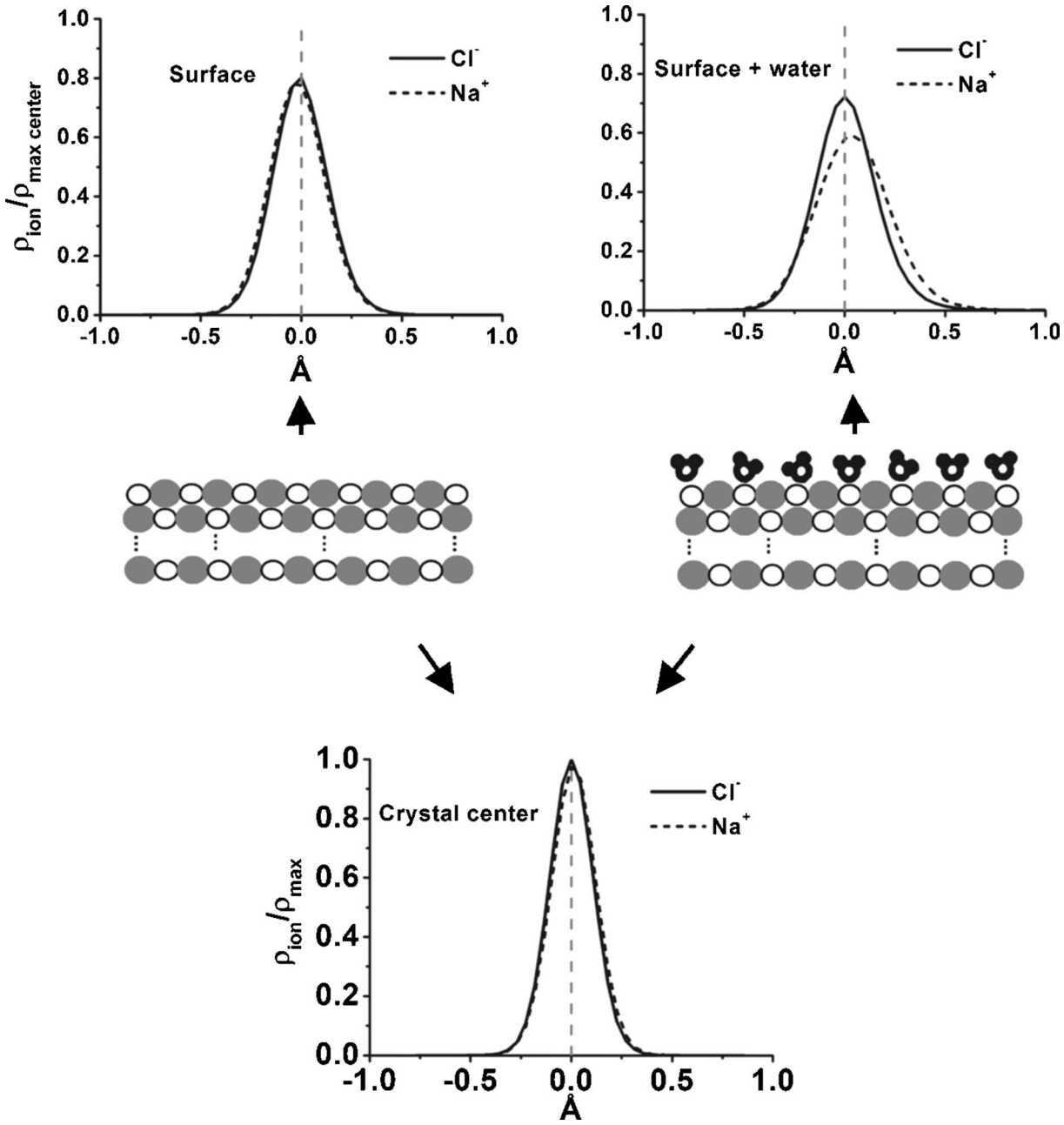

FIG. 7. Results of molecular dynamics simulations for the water/NaCI interface. The graphs represent calculated ion density profiles. A slight upwards displacement from the lattice is obtained in the presence of water (top right). Without water no such a shift was observed (top left). The bottom graph corresponds to the ionic profiles in the bulk.

B. The origin of the surface-potential changes due to water adsorption in melt-grown NaCl crystals

Studies of water adsorption on NaCl by infrared adsorption spectroscopy concluded that the first monolayer of adsorbed water is completed at around 40% RH.[6] This point is very close to the RH value where the contact potential becomes uniform over the entire surface, suggesting that these two results are related. The increasingly negative value of the average contact potential is a clear indication that negative charges, or dipoles pointing down towards the surface, are being generated by water adsorption. It is known that the water molecules adsorb preferentially on the positive ions.[18] Density Functional Theory (DFT)[19] and *ab initio* molecular-dynamics (MD)[20] calculations show that for a coverage of one monolayer, water adsorption is favored on top of the Na ions. The most favorable geometry has the molecular plane parallel to the surface. Classical Monte Carlo[21] and MD[22] simulations of water on NaCl (100) also show that the water molecules bind to the Na ions through the oxygen end and with the molecular plane parallel to the surface or tilted slightly upwards. These water configurations could create a small positive surface dipole, which cannot account for our observed changes in contact potential.

Another possible effect of water adsorption is a rearrangement or relaxation of surface ions, where Na or Cl could move relative to the surface plane. To check this possibility we performed a classical MD simulation on a system consisting of a NaCl slab of $8\times8\times5$ unit cells with a layer

of 128 water molecules on the top face at room temperature. Fixed charge simple extended point charge (SPC)/*E* potentials were used for water and Born-Huggins-Mayer potentials for the NaCl, as in a recent simulation of water adsorption at NaCl steps.[23] Using this model we found that water molecules adsorb preferentially on the sodium ions but also form clusters, as has been reported for previous calculations with similar potentials.[24] We focus on the z coordinates of ions in the plane in contact with the water molecules and compare this to the dry surface. The density profiles of both sodium and chloride ions have been calculated for each lattice plane.

The results are shown in Fig. 7. The density profile of the sodium ions is wider and centered at a higher z value, indicating that sodium moves up from the lattice plane as a result of the interaction with water molecules. This should again produce a positive dipole on the surface, contrary to the observations. There are more complex potentials for water molecules that take into account the possibility of polarization of the molecules when interacting with other molecules. These models do not show significant structural differences from the type of potentials used in this study[21,22] for a water coverage of one monolayer. The more complex models might change the magnitude of the sodium ion relaxation, but it is unlikely that they reverse the direction. We therefore conclude that the observed negative surface potential is due to be the preferential detachment and solvation of chloride ions from the steps in the presence of water. These ions are then free to diffuse in response to the electric field from the tip, accounting for both the decrease of surface potential and the increase in polarizability.

C. Ionic mobility and frequency response

Although frequency-dependent effects are only visible in the images above 30% RH, some limited ionic mobility must already be present for RH as low as 20% to explain the reduction in contact potential variations on the terraces and the step rounding observed at this low humidity (Fig. 3).

In our models the concentration of solvated anions is very small at low RH. The attractive force between these anions and the lattice cations around the vacancy is strong enough to keep the solvated anions close to their initial position. Because it is easier to remove atoms from a step edge than from a terrace, it is not surprising that the steps are more charged. As the density of solvated Cl^- ions increases, their mutual repulsion facilitates motion away from their original sites and migration onto the terraces. This process helps to equalize the contact potential of steps and terraces.

The mobility of the solvated anions localized near steps leads to enhanced step polarizability and explains the large step enhancement observed in the SPFM images. This enhancement is at first limited to the steps but then spreads to the terraces as humidity increases towards 40% RH.

Although we have based this discussion on the solvation of Cl^- ions, it is clear that positive Na ions are also solvated to a lesser extent. This is evident from the observed rounding of initially straight cleavage steps. The very rapid motion of steps for RH above 40% provides further evidence for both anion and cation solvations.

V. SUMMARY AND CONCLUSIONS

We have used SPFM to study the evolution of surface potential and ionic mobility on NaCl surfaces as a function of relative humidity from 10% to close to 40%. We have gained a better understanding of the first stages of water adsorption on the NaCl surface. The NaCl surface produced by cleavage of melt-grown crystals at low humidity (10%) shows an average negative contact potential, after allowing for the compensation of the charge imbalance produced by cleavage, which can be positive or negative. The average surface potential becomes more negative as humidity increased, a result explained by the solvation of negative chloride ions from the lattice. Molecular-dynamic simulations predict a relaxation of cations, creating a positive dipole, however, this effect appears to be overwhelmed by anion solvation.

The solvated chloride ions are mobile on the surface on a millisecond time scale and are responsible for the rapid increase in the surface polarizibility. This polarizability is nonuniform below 40% RH and is higher at the steps. We have also shown that electrostatic effects, manifested in changes in the surface-potential distribution, are very sensitive to NaCl crystal purity. High-purity melt-grown crystals exhibit a general decrease of surface potential, which become more negative as the humidity increases. The less pure natural crystals used in this study exhibited an opposite effect, with the surface potential becoming more positive, at least up to the critical humidity of 40% above which large scale step motions and ionic redistribution take place.

ACKNOWLEDGMENTS

The authors would like to thank J. J. Sáenz and S. Ghosal for interesting discussions. This work was supported by the Director, Office of Energy Research, Office of Basic Energy Sciences, Materials Sciences Division of the U.S. Department of Energy under Contract No. DE-AC03-76SF00098. Two of the authors (A.V. and G.M.S.) acknowledge financial support from the Spanish Ministry of Science and Education.

[1] S. Yu. Sedunov, *Physics of Drop Formation in the Atmosphere* (Wiley, New York, 1974).
[2] E. M. Knipping, M. J. Lakin, K. L. Foster, P. Jungwirth, D. J. Tobias, R. B. Gerber, D. Dabdub, and B. J. Finlayson-Pitts, Science **288**, 301 (2000); R. Sander, W. C. Keene, A. A. Pszenny, *et al.*, Atmos. Chem. Phys. **3**, 1301 (2003).
[3] Q. Dai, J. Hu, and M. Salmeron, J. Phys. Chem. B **101**, 1994 (1997).
[4] M. Luna, F. Rieutord, N. A. Melman, Q. Dai, and M. Salmeron, J. Phys. Chem. A **102**, 6793 (1998).
[5] M. Hucher, A. Oberlin, and R. Hocart, Bull. Soc. Fr. Mineral. Cristallogr. **90**, 320 (1967).
[6] S. J. Peters and G. E. Ewing, Langmuir **13**, 6345 (1997); M. C. Foster and G. E. Ewing, J. Chem. Phys. **112**, 6817 (2000).
[7] S. Ghosal, A. Verdaguer, J. C. Hemminger, and M. Salmeron, J. Phys. Chem. A **109**, 4744 (2005).
[8] J. Hu, X.-D. Xiao, D. F. Ogletree, and M. Salmeron, Science **268**, 267 (1995).
[9] J. Hu, X.-D. Xiao, D. F. Ogletree, and M. Salmeron, Appl. Phys. Lett. **67**, 476 (1995).
[10] S. Gómez-Moñivas, L. S. Froufe-Perez, A. J. Caamano, and J. J. Saenz, Appl. Phys. Lett. **79**, 4048 (2001).
[11] L. Xu, A. Lio, J. Hu, D. F. Ogletree, and M. Salmeron, J. Phys. Chem. B **102**, 540 (1998).

[12] S. Gómez-Moñivas, J. J. Sáenz, R. Carminati, and J. J. Greffet, Appl. Phys. Lett. **76**, 2955 (2000).
[13] C. Schonenbergher and S. F. Alvarado, Phys. Rev. Lett. **65**, 3162 (1990); U. H. Yokohama and T. Inoue, Thin Solid Films **242**, 33 (1994).
[14] H. Bluhm, S. H. Pan, L. Xu, T. Inoue, D. F. Ogletree, and M. Salmeron, Rev. Sci. Instrum. **69**, 1781 (1998).
[15] SPI supplies, West Chester PA.
[16] L. B. Harris and J. Fiasson, J. Phys. C **18**, 4845 (1985).
[17] M. Tanibayashi, J. Phys. Soc. Jpn. **63**, 168 (1994); J. Frenkel, *Theory of Liquids* (Oxford University Press, Oxford, 1946 p. 36;) J. D. Eshelby, C. W. A. Newey, P. L. Pratt, and A. B. Lidiard, London, Edinburgh Dublin Philos. Mag. J. Sci. 3, 75 (1958).
[18] P. B. Barraclough and P. G. Hall, Surf. Sci. **46**, 393 (1974).
[19] J. M. Park, J.-H. Cho, and K. S. Kim, Phys. Rev. B **69**, 233403 (2004).
[20] M. Hendrik, P. Entel, and J. Hafner, Surf. Sci. **488**, 177 (2001).
[21] O. Engvist and A. J. Stone, J. Chem. Phys. **110**, 12089 (1999).
[22] E. Stockelmann and R. Hentschke, J. Chem. Phys. **110**, 12097 (1999).
[23] S. Garcia-Manyes, A. Verdaguer, P. Gorostiza, and F. Sanz, J. Chem. Phys. **120**, 2962 (2004).
[24] O. Engkvist and A. J. Stone, J. Chem. Phys. **112**, 6827 (2000).